General Model and Analysis of Misalignment Characteristics of Fixed-Frequency WPT Systems

Yixiang Yao and Wenxing Zhong, *Senior Member, IEEE*

***Abstract*—To obtain a smooth output of a wireless power transfer (WPT) system over a large-misalignment range, many efforts have been devoted to altering compensating parameters of conventional compensating topologies, such as series–series, *LCC–LCC*, and proposing new compensating topologies, which naturally have better misalignment performance, such as *CCC* and X-type. This article shows that these systems, with fixed operating frequencies and optimized misalignment performance, can be described with the same mathematical model. The model is first introduced. Then, based on this model, a general analysis on the misalignment performance of two- and multicoil WPT systems is provided. According to the output-misalignment characteristics, these systems are divided into two groups, i.e., low degree and high degree. A detailed analysis of the low-degree WPT system is performed, with either a resistive load or a battery load. It is found that most (if not all) of the reported large-misalignment WPT systems are low-degree systems and they have a similar misalignment performance. Moreover, a general design method of the compensating networks is presented for lower degree WPT systems to achieve the desired misalignment performance. As an example, the compensating networks of a two-coil WPT system are designed and the experimental results verify the proposed model and the design method.**

***Index Terms*—General analysis, misalignment characteristic, wireless power transfer (WPT).**

I. Introduction

THE development of wireless power transfer (WPT) technology for wireless charging of consumer electronics and electric vehicles (EVs) is the motivation behind many exceptional studies. EV WPT systems must possess high misalignment tolerance, which is a critical performance metric [1]. In order to improve the misalignment characteristic, many methods have been proposed, e.g., misalignment-tolerated structures for couplers [2], [3], [4] and control method to compensate the effect caused by misalignment [5]. Previous research has identified a category of methods that utilize well-designed topologies to attain favorable misalignment characteristics without modifying frequency or employing misalignment-compensated controls [6]. This type of WPT system is named as the fixed-frequency WPT system in this article. The absence of a misalignment-compensated controller results in a simpler and more cost-effective WPT system. Alternatively, even if a misalignment-compensated controller is included, this class of topologies can help improve the misalignment performance and extend the misalignment range.

For fixed-frequency WPT systems, several articles have proposed methods to improve misalignment tolerance by modifying component values in the conventional WPT system topologies. These modifications include detuning a series–series (SS) WPT system [7], modifying the parameters of *LCC*-S [8], [9], [10], S-SP [11], PS-S [12], and *LCC–LCC* and S-*LCC* topologies [13]. In addition to modifying the component values of the conventional WPT system topologies, a few novel compensation topologies to improve misalignment tolerance have been proposed, including X-type [14], *CCC* [15], and S-*CLC* [16]. Some articles have also explored the use of multicoil systems, such as a three-coil system, to improve the misalignment performance of a WPT system [17].

Among these studies on fixed-frequency WPT systems, we find that the misalignment characteristics of these misalignment-enhanced WPT systems are highly similar. Specifically, as the misalignment increases, the output power of such a WPT system initially increases and then decreases. Additionally, a larger misalignment distance leads to larger power fluctuation. This article introduces a unified model and theory for fixed-frequency WPT systems, which reveals the shared mathematical characteristics of these topologies, highlighting their low-degree misalignment characteristics (LDMC). Moreover, the article identifies that coaxial multicoil-to-multicoil WPT systems exhibit high-degree misalignment characteristics (HDMC). This discovery holds the potential for groundbreaking advancements in misalignment characteristics of fixed-frequency WPT systems. Additionally, the article presents an analytical approach that combines misalignment range, output power fluctuations, and inverter volt-ampere (VA) rating. This methodology allows for the direct determination of system parameters, eliminating the need for numerical optimization methods. Consequently, the design process for the LDMC-WPT system is significantly simplified. Furthermore, for the battery loads commonly utilized in WPT systems, this study also shows that power fluctuation caused by misalignment can be further reduced compared with the system with resistive loads. A design method to minimize power fluctuations, in this case, is provided.

The rest of this article is organized as follows. In Section II, circuit and mathematical models are developed for

Manuscript received 27 February 2023; revised 23 June 2023; accepted 30 July 2023. Date of publication 4 August 2023; date of current version 22 September 2023. Recommended for publication by Associate Editor G. Anthony. *(Corresponding author: Wenxing Zhong.)*

The authors are with the Institute of Power Electronics, Zhejiang University, Hangzhou 310027, China (e-mail: 12110008@zju.edu.cn; wxzhong@zju.edu.cn).

Color versions of one or more figures in this article are available at https://doi.org/10.1109/TPEL.2023.3301655.

Digital Object Identifier 10.1109/TPEL.2023.3301655

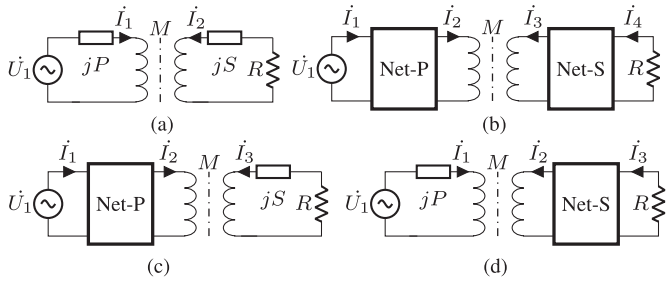

Fig. 1. General circuits of the two-coil WPT systems with different numbers of current loops. (a) 1-1-loop, (b) 2-2-loop, (c) 2-1-loop, and (d) 1-2-loop.

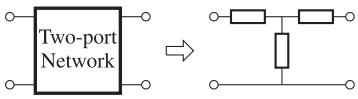

Fig. 2. Passive two-port network is equivalent to a T-type circuit.

two- and multicoil coaxial WPT systems. In Section III-A, the general output current-misalignment characteristics of fixed-frequency WPT systems are deduced, from which they are divided into two groups, i.e., LDMC- and HDMC-WPT systems. In Sections III-B–D, three important misalignment characteristics are derived. In Section III-E, several previous studies [8], [11], [13], [14], [15], [17] are integrated into the theory of this article. In Section IV, a two-coil prototype is designed, and in Section V, the experimental results are presented to verify the theoretical analysis. Finally, Section VI concludes this article.

II. General Modeling of Fixed-Frequency WPT Systems

A. Model of Two-Coil WPT System

Fig. 1 shows the general circuit diagrams of two-coil WPT systems, which can be divided into four different types. In these circuits, M is the mutual inductance; $\dot{U}_1$ is the input voltage; and R is the load resistance. The difference among these four circuits is the current loop. Fig. 1(a) shows the SS-compensated WPT system, which includes two current loops. P and S are the reactances of the primary and secondary sides, respectively. In Fig. 1(b), (c), and (d), Net-P and Net-S are two-port networks at the primary and secondary sides, respectively. A passive two-port network, which contains more than one current loop, can be equivalent to a T-type circuit [18], as shown in Fig. 2. Therefore, for the circuit in Fig. 1(c), there are two current loops at the primary side, similarly for Fig. 1(b) and (d).

In WPT systems, compensation circuits are usually formed by capacitors and inductors. In this study, the inductances of the power transfer coils are included in P, S, Net-P, or Net-S. For two-port networks Net-P and Net-S, they can be described with the general equation given as

$$\dot{\boldsymbol{U}} = \boldsymbol{Z}_{\mathrm{P/S}}\dot{\boldsymbol{I}} \tag{1}$$

where $\dot{\boldsymbol{U}}$ and $\dot{\boldsymbol{I}}$ are the voltage vector and current vector of two ports, respectively, and $\boldsymbol{Z}_{\mathrm{P/S}}$ is the impedance matrices. The

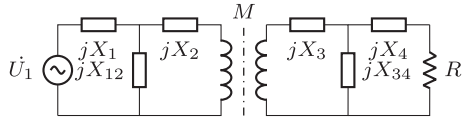

Fig. 3. Circuit model of the two-coil WPT system with four current loops.

general format of the impedance matrices of Net-P and Net-S are given as follows:

$$\boldsymbol{Z}_{\mathrm{P}} = \begin{bmatrix} jP_{00} & jP_{01} \\ jP_{01} & jP_{11} \end{bmatrix}, \quad \boldsymbol{Z}_{\mathrm{S}} = \begin{bmatrix} jS_{11} & jS_{01} \\ jS_{01} & jS_{00} \end{bmatrix} \tag{2}$$

where P_{ij} and S_{ij} are the real numbers.

For example, Fig. 3 shows a 2-2-loop WPT system. The components in Z_{P} and Z_{S} of this system can be derived as

$$P_{00} = X_1 + X_{12},\ P_{01} = -X_{12},\ P_{11} = X_{12} + X_2$$
$$S_{11} = X_3 + X_{34},\ S_{01} = -X_{34},\ S_{00} = X_{34} + X_4. \tag{3}$$

The loop circuit equation of the four types of two-coil WPT systems in Fig. 1 can be expressed as

$$\begin{bmatrix} \dot{U}_1 \\ 0 \end{bmatrix} = \left[\begin{array}{c|c} jP & xj\omega M \\ \hline xj\omega M & jS + R \end{array}\right] \begin{bmatrix} \dot{I}_1 \\ \dot{I}_2 \end{bmatrix} \tag{4a}$$

$$\begin{bmatrix} \dot{U}_1 \\ 0 \\ 0 \end{bmatrix} = \left[\begin{array}{cc|c} jP_{00} & jP_{01} & 0 \\ jP_{01} & jP_{11} & xj\omega M \\ \hline 0 & xj\omega M & jS + R \end{array}\right] \begin{bmatrix} \dot{I}_1 \\ \dot{I}_2 \\ \dot{I}_3 \end{bmatrix} \tag{4b}$$

$$\begin{bmatrix} \dot{U}_1 \\ 0 \\ 0 \end{bmatrix} = \left[\begin{array}{c|cc} jP & xj\omega M & 0 \\ \hline xj\omega M & jS_{11} & jS_{01} \\ 0 & jS_{01} & jS_{00} + R \end{array}\right] \begin{bmatrix} \dot{I}_1 \\ \dot{I}_2 \\ \dot{I}_3 \end{bmatrix} \tag{4c}$$

$$\begin{bmatrix} \dot{U}_1 \\ 0 \\ 0 \\ 0 \end{bmatrix} = \left[\begin{array}{cc|cc} jP_{00} & jP_{01} & 0 & 0 \\ jP_{01} & jP_{11} & xj\omega M & 0 \\ \hline 0 & xj\omega M & jS_{11} & jS_{01} \\ 0 & 0 & jS_{01} & jS_{00} + R \end{array}\right] \begin{bmatrix} \dot{I}_1 \\ \dot{I}_2 \\ \dot{I}_3 \\ \dot{I}_4 \end{bmatrix} \tag{4d}$$

where $\dot{I}_i$ is the current in the ith loop. To investigate the misalignment performance of the systems, a misalignment coefficient x is introduced, which is defined as the ratio of the mutual inductance at the misaligned position to the aligned position. In a usual WPT system, the self-inductances of the coils do not vary much with the misalignment. Therefore, in this study, they are treated as constants.

Equation (4) can be unified in the form of

$$\dot{\boldsymbol{U}} = \boldsymbol{Z}_{1\sim1}\dot{\boldsymbol{I}} \tag{5}$$

where subscript $1\sim1$ means single coil to single coil. $\boldsymbol{Z}_{1\sim1}$ can be divided into four block matrices, i.e.,

$$\boldsymbol{Z}_{1\sim1} = \left[\begin{array}{c|c} \boldsymbol{P} & \boldsymbol{M} \\ \hline \boldsymbol{M}^{\mathrm{T}} & \boldsymbol{S} \end{array}\right]. \tag{6}$$

B. Model of Coaxial Multicoil WPT System

The model of two-coil WPT systems can be extended to coaxial multicoil WPT systems. Fig. 4 shows the general circuit

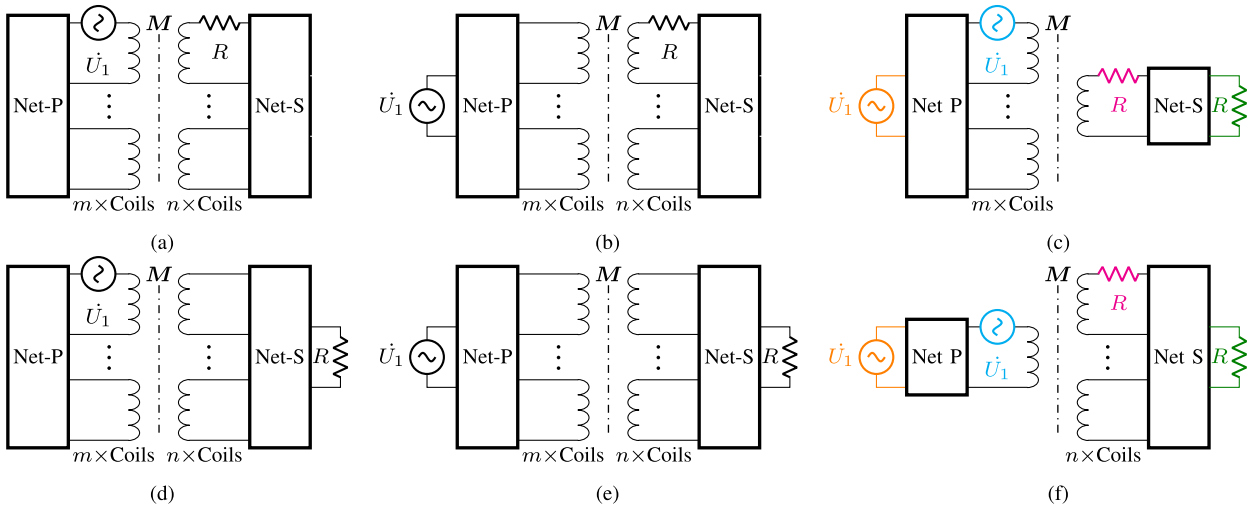

Fig. 4. General circuits of multicoil-to-multicoil WPT systems: (a) $m-n$-loop, (b) $(m+1)-n$-loop, (d) $m-(n+1)$-loop, (e) $(m+1)-(n+1)$-loop; (c) multicoil-to-single-coil WPT systems; and (f) single-coil-to-multicoil WPT systems [note that the colored voltage sources and load resistors in (c) and (f) represent possiblelocations, encompassing the cases in (a), (b), (d), and (e)].

diagram of multicoil-to-multicoil systems. There are m and n coils on the primary and the secondary side, respectively. It should be noted that any two of the coils on the same side are not connected in series. Because two series coils can be essentially considered as one in circuit analysis. In Fig. 4, if the input voltage source is in series with one of the primary coils, Net-P is an m-port network, as shown in Fig. 4(a) and (d); otherwise, it is an (m+1)-port network, as shown in Fig. 4(b) and (e). Similarly, the load resistor R also has two different connections. As a result, the topologies of the multicoil WPT systems are divided into four different types, i.e., m-n-loop, (m+1)-n-loop, m-(n+1)-loop, and (m+1)-(n+1)-loop. The inductances of the coils and the mutual inductances between two coils on the same side are included in Net-P or Net-S.

The circuit equations of the multicoil-to-multicoil WPT system in Fig. 4 are given by

$$\dot{\boldsymbol{U}} = \boldsymbol{Z}_{m\sim n}\dot{\boldsymbol{I}} \tag{7}$$

where $\boldsymbol{Z}_{m\sim n}$ is the impedance matrix of the multicoil WPT system, as given in (9) shown at the bottom of the next page, and

$$\dot{\boldsymbol{U}} = [\dot{U}_1, 0, \ldots, 0]^{\mathrm{T}}, \qquad \dot{\boldsymbol{I}} = [\dot{I}_1, \dot{I}_2, \ldots, \dot{I}_K]^{\mathrm{T}} \tag{8}$$

where K is the total number of all loops in the WPT system. In $\boldsymbol{Z}_{m\sim n}$, M_{ij} is the mutual inductance between the ith coil at the primary side and the jth coil at the secondary side. In the following analysis, it is assumed that all the mutual inductances of two different-side coils change at the same rate, which is described with the misalignment coefficient x. This assumption is valid if the coils on the same side are coaxial, as shown in Fig. 5, and the misalignment is within a reasonable range with respect to the size of the coils. Different topologies in Fig. 4 will have different $\boldsymbol{Z}$ matrices. For the m-n-loop system, $\boldsymbol{Z}_{m\sim n}$ is in the light purple block in (9), and for the (m+1)-n-loop system, $\boldsymbol{Z}_{m\sim n}$ is in the light cyan block, with load resistor R added after jS_{11} in both cases. For the m-(n+1)-loop system, $\boldsymbol{Z}_{m\sim n}$ is in the light magenta block, and for (m+1)-(n+1)-loop system, $\boldsymbol{Z}_{m\sim n}$ is the whole matrix, with load resistor R added after jS_{00} in both cases.

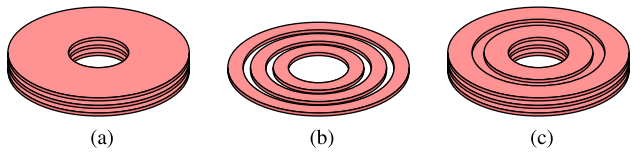

Fig. 5. Pad structure of coaxial multicoil WPT systems. (a) Stacked structure. (b) Concentric structure. (c) Hybrid structure.

III. Analysis of Misalignment Characteristics

A. General Output Current-Misalignment Characteristics

According to (7), it can be derived that

$$\dot{\boldsymbol{I}} = \boldsymbol{Z}_{m\sim n}^{-1}\dot{\boldsymbol{U}}. \tag{10}$$

The last column of (10) is

$$\dot{I}_K = Z_{(K1)}^{-1}\cdot\dot{U}_1 \tag{11}$$

where $Z_{(K1)}^{-1}$ represents the element at the lower left corner of matrix $\boldsymbol{Z}_{m\sim n}^{-1}$, and $Z_{(K1)}^{-1}$ can be calculated as

$$Z_{(K1)}^{-1} = \frac{\det(\boldsymbol{A}_{1K})}{\det(\boldsymbol{Z}_{m\sim n})} \tag{12}$$

where $\boldsymbol{A}_{1K}$ is the algebraic cofactor matrix of the element in the upper right corner of $\boldsymbol{Z}_{m\sim n}$, and $\det(\boldsymbol{A}_{1K})$ and $\det(\boldsymbol{Z}_{m\sim n})$ represent the determinants of the matrices. The expressions of $\det(\boldsymbol{A}_{1K})$ and $\det(\boldsymbol{Z}_{m\sim n})$ are derived in Appendix A as

$$\det(\boldsymbol{A}_{1K}) = j^{(K-1)}\sum_{l=0}^{\min(m,n)-1} e_{(2l+1)}x^{(2l+1)} \tag{13}$$

$$\det\left(\boldsymbol{Z}_{m\sim n}\right)=\sum_{l=0}^{\min(m,n)}\left(a_{2l}+jb_{2l}\right)x^{2l} \tag{14}$$

where a_i, b_i, and e_i are the real numbers.

For the two-coil WPT systems, as shown in Fig. 1, as well as the multicoil-to-single-coil and the single-coil-to-multicoil WPT systems, as shown in Fig. 4(c) and (f), respectively, $\min(m,n)$ in (13) and (14) equals 1, so $Z_{(K1)}^{-1}$ has the following form:

$$Z_{(K1)}^{-1}=\frac{j^{(K-1)}e_1x}{(a_2+jb_2)x^2+(a_0+jb_0)}. \tag{15}$$

Such systems are considered to have LDMC. The multicoil-to-multicoil WPT systems satisfy $\min(m,n)\geq 2$, which are considered to have HDMC.

For example, for the 2-2-loop WPT system, as shown in Fig. 3, the expression of $Z_{(K1)}^{-1}$ is deduced in (16) shown at the bottom of this page, which satisfies the form of (15). By comparing it with (15), a_2, a_0, b_2, b_0, and e_1 can be obtained as follows:

$$\begin{aligned}
a_2&=-\omega^2M^2(X_1+X_{12})\left(X_4+X_{34}\right)\\
a_0&=(X_2X_{12}+X_1X_2+X_1X_{12})(X_4X_{34}+X_3X_4+X_3X_{34})\\
b_2&=\omega^2M^2(X_1+X_{12})\,R\\
b_0&=-\left(X_2X_{12}+X_1X_2+X_1X_{12}\right)(X_3+X_{34})R\\
e_1&=-\omega MX_{12}X_{34}.
\end{aligned} \tag{17}$$

The rest of this article focuses on WPT systems with LDMC, which are termed LDMC-WPT systems for short.

B. Output Power-Misalignment Characteristics With Resistive Load

This section further deduces the output power-misalignment characteristics. For resistive load, the output power is proportional to the square of I_K, and therefore

$$P=I_K^2R=\left\|Z_{(K1)}^{-1}\right\|^2U_1^2R. \tag{18}$$

Define a power-related coefficient $p_R(x)$ as

$$\begin{aligned}
p_R(x)&=\left\|Z_{(K1)}^{-1}\right\|^2\\
&=\frac{e_1^2}{\left(a_2^2+b_2^2\right)x^2+2\left(a_0a_2+b_0b_2\right)+\left(a_0^2+b_0^2\right)x^{-2}}.
\end{aligned} \tag{19}$$

In the denominator of (19), x^2 is an increasing function, and x^{-2} is a decreasing function. As a consequence, in the certain x range, the changing speed of $p(x)$ is reduced. By designing the compensation components of a WPT system to make this domain falls within the desired misalignment range, the misalignment performance of this system can be improved.

In this article, the output power of a WPT system at the aligned position (i.e., $x=1$) and the most misaligned position (i.e., $x=x_{\min}$) are considered the same, then

$$p(1)=p(x_{\min}). \tag{20}$$

From (20), $x_{\min}$ can be solved as

$$x_{\min}^2=\frac{a_0^2+b_0^2}{a_2^2+b_2^2}. \tag{21}$$

Then, (19) can be rewritten as

$$p_R(x)=\frac{e_1^2}{a_2^2+b_2^2}\cdot\frac{1}{x^2+2\lambda x_{\min}+x_{\min}^2\cdot x^{-2}} \tag{22}$$

where λ is a coefficient given by

$$\lambda=\frac{1}{x_{\min}}\cdot\frac{a_0a_2+b_0b_2}{a_2^2+b_2^2}. \tag{23}$$

From (22), it can be seen that the shape of function $p_R(x)$ is only related to $x_{\min}$ and λ. With (21) and (23), one can derive

$$x_{\min}^2-\left(\lambda x_{\min}\right)^2=x_{\min}^2\left(1-\lambda\right)^2=\left(\frac{a_2b_0-a_0b_2}{a_2^2+b_2^2}\right)^2\geq 0. \tag{24}$$

Thus, the range of λ is $(-1,1)$.

$$\boldsymbol{Z}_{m\sim n}=\left[\begin{array}{cccc|ccc|c}
jP_{00} & jP_{01} & \cdots & jP_{0m} & 0 & \cdots & 0 & 0\\
jP_{01} & jP_{11} & \cdots & jP_{1m} & xj\omega M_{1n} & \cdots & xj\omega M_{11} & 0\\
\vdots & \vdots & \ddots & \vdots & \vdots & \ddots & \vdots & \vdots\\
jP_{0m} & jP_{1m} & \cdots & jP_{mm} & xj\omega M_{mn} & \cdots & xj\omega M_{m1} & 0\\
\hline
0 & xj\omega M_{1n} & \cdots & xj\omega M_{mn} & jS_{nn} & \cdots & jS_{1n} & jS_{0n}\\
\vdots & \vdots & \ddots & \vdots & \vdots & \ddots & \vdots & \vdots\\
0 & xj\omega M_{11} & \cdots & xj\omega M_{m1} & jS_{1n} & \cdots & jS_{11}+(R) & jS_{01}\\
0 & 0 & \cdots & 0 & jS_{0n} & \cdots & jS_{01} & jS_{00}+(R)
\end{array}\right] \tag{9}$$

$$Z_{(41)}^{-1}=\frac{j\omega MX_{12}X_{34}\cdot x}{\omega^2M^2(X_1+X_{12})[-(X_4+X_{34})+jR]x^2+(X_2X_{12}+X_1X_2+X_1X_{12})[X_4X_{34}+X_3X_4+X_3X_{34}-j(X_3+X_{34})R]} \tag{16}$$

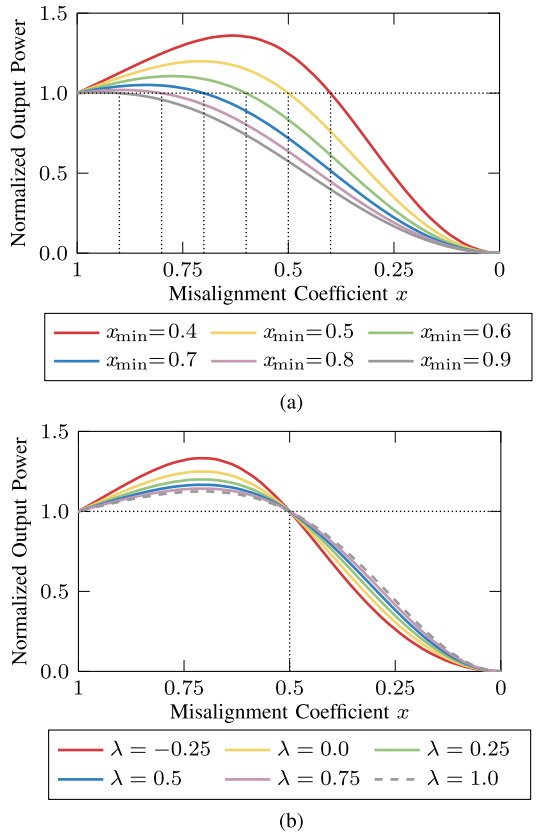

Fig. 6. Normalized output power-misalignment characteristics of the LDMC-WPT systems with resistive load when (a) $\lambda = 0.25$ with different $x_{\min}$, and (b) $x_{\min} = 0.5$ with different λ.

According to (22), the maximum value of $p(x)$ is given by

$$p_R(x) = \frac{e_1^2}{a_2^2 + b_2^2} \cdot \frac{1}{2x_{\min}(\lambda + 1)}. \tag{25}$$

Define a fluctuation coefficient κ_R as the ratio of the maximum output power to the output power at the aligned position. According to (22) and (25), κ_R is given by

$$\kappa_R(x_{\min}, \lambda) = \frac{x_{\min}^2 + 2\lambda x_{\min} + 1}{2(1+\lambda)x_{\min}}. \tag{26}$$

Fig. 6(a) and (b) show how $x_{\min}$ and λ affect the output power-misalignment characteristics of an LDMC-WPT system, respectively, where the output power is normalized to the output power at $x = 1$. In the figures, it can be observed that when λ remains constant, if a larger misalignment range is required (i.e., a smaller $x_{\min}$), it leads to greater fluctuation in the output power. This fluctuation can be reduced by increasing λ.

C. Input Current-Misalignment Characteristics With Resistive Load

This section deduces the input current-misalignment characteristics, whichare correlated with the VA rating of the inverter. The first row of (10) is

$$\dot{I}_1 = Z_{(11)}^{-1} \cdot \dot{U}_1 \tag{27}$$

where I_1 is the input current, and $Z_{(11)}^{-1}$ represents the element at the upper left corner of matrix $\boldsymbol{Z}_{m\sim n}^{-1}$. Similar to (12), $Z_{(11)}^{-1}$ can be calculated as

$$Z_{(11)}^{-1} = \frac{\det(\boldsymbol{A}_{11})}{\det(\boldsymbol{Z}_{m\sim n})} \tag{28}$$

where $\boldsymbol{A}_{11}$ is the algebraic cofactor matrix of the element in the upper left corner of $\boldsymbol{Z}_{m\sim n}$.

It is proved in Appendix B that for the LDMC-WPT system, $Z_{(11)}^{-1}$ has the following form:

$$Z_{(11)}^{-1} = \frac{jc_2(a_2 + jb_2)x^2 + jc_0(a_0 + jb_0)}{(a_2 + jb_2)x^2 + (a_0 + jb_0)} \tag{29}$$

where a_i, b_i, and c_i are the real numbers, and if there is only one current loop at the primary side, then $c_2 = 0$. For example, for the 2-2-loop WPT system, as shown in Fig. 3, the expression of $Z_{(11)}^{-1}$ is deduced in (30) shown at the bottom of next page, which satisfies the form of (29) By defining the input current function $I_{\text{in}}(x)$ that equals $Z_{(11)}^{-1}$, (29) can be transformed into $(A + jB)$ form as

$$I_{\text{in}}(x) = \frac{(c_2 - c_0)(a_2b_0 - a_0b_2)x^2}{(a_2^2 + b_2^2)x^4 + 2(a_0a_2 + b_0b_2)x^2 + (a_0^2 + b_0^2)} + j\frac{c_2(a_2^2+b_2^2)x^4 + 2(c_2+c_0)(a_0a_2+b_0b_2)x^2 + c_0(a_0^2+b_0^2)}{(a_2^2 + b_2^2)x^4 + 2(a_0a_2 + b_0b_2)x^2 + (a_0^2 + b_0^2)}. \tag{31}$$

In the design stage, zero phase angle (ZPA) is normally guaranteed in either the aligned position or the most misaligned position. Suppose ZPA is realized at the aligned position, including (21) and (23), the following equation can be deduced:

$$c_2 + 2(c_2 + c_0)\lambda x_{\min} + c_0 x_{\min}^2 = 0. \tag{32}$$

Similarly, if the ZPA point is realized at the most misaligned position, the following equation can be deduced:

$$c_2 x_{\min}^2 + 2(c_2 + c_0)\lambda x_{\min} + c_0 = 0. \tag{33}$$

It should be noted that for LDMC-WPT systems with only one current loop at the primary side, c_2 in (32) and (33) equals zero, then it can be deduced from (32) and (33) that

$$\lambda = -\frac{x_{\min}}{2} \quad \text{or} \quad \lambda = -\frac{1}{2x_{\min}}. \tag{34}$$

This means that for such systems, $x_{\min}$ and λ need to meet the above equations to achieve ZPA at either $x = 1$ or $x = x_{\min}$.

According to (24)

$$\frac{a_2b_0 - a_0b_2}{a_2^2 + b_2^2} = \pm\sqrt{x_{\min}^2 - \lambda^2 x_{\min}^2}. \tag{35}$$

Substituting (21), (23), (32), and (35) into (31), the general input current-misalignment characteristic of the LDMC-WPT system with ZPA at the aligned and misaligned positions can be, respectively, deduced as follows:

$$I_{\text{in}}(x) = |c_2| \left\{ \frac{x^2\left(x_{\min}^2 + 2\lambda x_{\min} + 1\right) x_{\min}\sqrt{1-\lambda^2}}{(x_{\min}^2 + \lambda x_{\min})(x^4 + 2\lambda x_{\min} x^2 + x_{\min}^2)} \right.$$

$$\pm j\,\frac{(1-x^2)\left[\left(\lambda x_{\min}+x_{\min}^2\right)x^2+\left(\lambda x_{\min}^3+x_{\min}^2\right)\right]}{\left(x_{\min}^2+\lambda x_{\min}\right)\left(x^4+2\lambda x_{\min}x^2+x_{\min}^2\right)}\Bigg\} \tag{36}$$

$$I_{\text{in}}(x)=|c_2|\left\{\frac{x^2\left(x_{\min}^2+2\lambda x_{\min}+1\right)x_{\min}\sqrt{1-\lambda^2}}{\left(1+\lambda x_{\min}\right)\left(x^4+2\lambda x_{\min}x^2+x_{\min}^2\right)}\right.$$
$$\left.\pm j\,\frac{\left(x^2-x_{\min}^2\right)\left[\left(\lambda x_{\min}+1\right)x^2+\left(\lambda x_{\min}+x_{\min}^2\right)\right]}{\left(1+\lambda x_{\min}\right)\left(x^4+2\lambda x_{\min}x^2+x_{\min}^2\right)}\right\}. \tag{37}$$

Fig. 7 shows how λ affects the input current-misalignment characteristic of the LDMC-WPT system. In Fig. 7, the amplitude of the input current is normalized to the value at the ZPA point. It should be emphasized that λ in (36) and (37) cannot equal to ± 1; otherwise, it will lead to the real part of the input current, which is equal to zero. If λ approaches 1, the input power will be unexpectedly large, as shown in the curve of $\lambda = 0.99$ in Fig. 7(a) and (b). Hence, the curve of $\lambda = 1.0$ in Fig. 6(b) is dashed to indicate that this curve is unavailable. As mentioned before, increasing λ can reduce output power fluctuations. However, it can be observed in Fig. 7 that as λ increases beyond a certain value, which is about 0.25 in this case study, the maximum input current will increase at an increasingly rapid pace. Therefore, a tradeoff should be made among misalignment range, output power fluctuation, and VA rating when designing such a WPT system.

D. Output Power-Misalignment Characteristic With Battery Load

This section studies the output power-misalignment characteristic with a battery load. Fig. 8(a) shows the Thevenin equivalent circuit of the WPT system without a load. In this circuit, $\dot{U}_{\text{oc}}$ is the open-circuit voltage. If the parasitic resistances of the compensation components are neglected, the equivalent impedance is a reactance X_{eq}, then

$$\dot{U}_{\text{oc}} = jX_{\text{eq}}\dot{I}_{\text{sc}} \tag{38}$$

where $\dot{I}_{\text{sc}}$ is the short-circuit current of the Thevenin equivalent circuit.

By neglecting the internal resistance, battery loads have two characteristics: the charging voltage is constant, and the charging voltage and the charging current are in phase. According to Fig. 8(b), the two characteristics can be described with the following equations:

$$\begin{cases} \left\|U_{\text{oc}}-jX_{\text{eq}}\dot{I}\right\| = U_{\text{cnt}} \\ \angle\left(U_{\text{oc}}-jX_{\text{eq}}\dot{I}\right) = \angle\dot{I} \end{cases} \tag{39}$$

where U_{cnt} is the constant battery voltage. Define P_{a} as the output power while a WPT system is at the aligned position. Then

$$U_{\text{cnt}} = \sqrt{P_{\text{a}}R}. \tag{40}$$

By solving (39), the expression of current $\dot{I}$ can be obtained as follows:

$$\dot{I} = \frac{\sqrt{U_{\text{cnt}}^2U_{\text{oc}}^2-U_{\text{cnt}}^4}}{|X_{\text{eq}}|\,U_{\text{oc}}} + j\frac{U_{\text{cnt}}^2-U_{\text{oc}}^2}{X_{\text{eq}}U_{\text{oc}}}. \tag{41}$$

Then, with (38), the power P_{DC} at this condition can be calculated as

$$P_{\text{DC}} = U_{\text{cnt}}\sqrt{\frac{I_{\text{sc}}^2\left(U_{\text{cnt}}^2-U_{\text{oc}}^2\right)}{U_{\text{oc}}^2}}. \tag{42}$$

It is proved in Appendix C that if the number of current loops is an even number, then

$$Z_{(K1)}^{-1} = \frac{j^{(K-1)}e_1x}{(a_2+j\beta_2R)x^2+(a_0+j\beta_0R)} \tag{43}$$

where a_0, a_2, β_0, and β_2 are independent of R, and

$$b_0 = \beta_0R, \quad b_2 = \beta_2R. \tag{44}$$

For example, for the 2-2-loop WPT system, as shown in Fig. 3, the expression of $Z_{(K1)}^{-1}$ in (16) satisfies the pattern of (43). And if the number of current loops is an odd number, then

$$Z_{(K1)}^{-1} = \frac{j^{(K-1)}e_1x}{(\alpha_2R+jb_2)x^2+(\alpha_0R+jb_0)} \tag{45}$$

where α_0, α_2, b_0, and b_2 are independent of R, and

$$a_0 = \alpha_0R, \quad a_2 = \alpha_2R. \tag{46}$$

The two cases mentioned above exhibit similarities; therefore, this article focuses solely on the analysis of WPT systems with even-numbered current loops, as the analysis of the other case is analogous.

If R equals zero, the short-circuit current I_{sc} can be derived as

$$I_{\text{sc}} = Z_{(K1)}^{-1}\Big|_{R=0}\cdot U_1 = \frac{j^{(K-1)}e_1xU_1}{a_2x^2+a_0}. \tag{47}$$

If R tends to infinity, the open-circuit voltage U_{oc} can be derived as

$$\begin{aligned} U_{\text{oc}} &= \lim_{R\to+\infty} Z_{(K1)}^{-1}\cdot U_1R \\ &= \lim_{R\to+\infty}\frac{j^{(K-1)}e_1xRU_1}{(a_2+j\beta_2R)x^2+(a_0+j\beta_0R)} \\ &= -\frac{j^Kxe_1U_1}{\beta_2x^2+\beta_0}. \end{aligned} \tag{48}$$

$$Z_{(11)}^{-1}=\frac{j\left(-\omega^2M^2\right)\left[-(X_4+X_{34})+jR\right]x^2+\quad j\left(-X_2-X_{12}\right)\left[(X_4X_{34}+X_3X_4+X_3X_{34})-j(X_3+X_{34})R\right]}{\omega^2M^2(X_1+X_{12})[-(X_4+X_{34})+jR]x^2+(X_2X_{12}+X_1X_2+X_1X_{12})[(X_4X_{34}+X_3X_4+X_3X_{34})-j(X_3+X_{34})R]}. \tag{30}$$

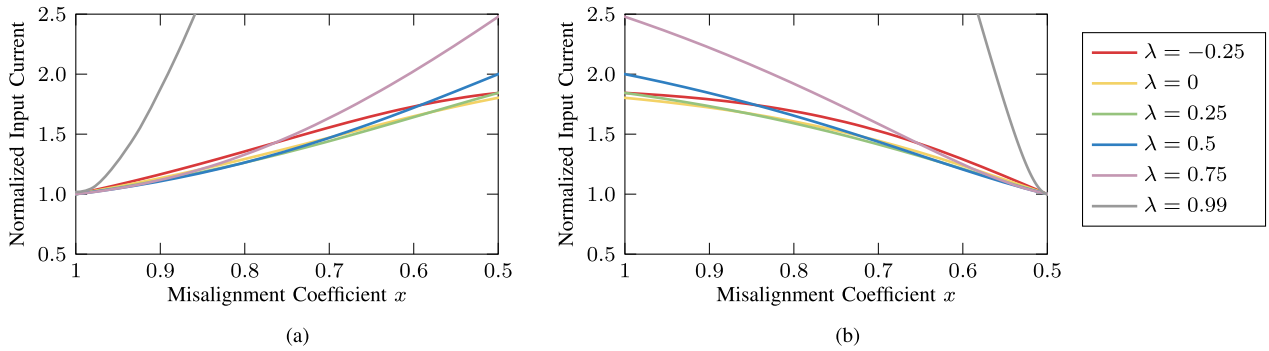

Fig. 7. Normalized input current-misalignment characteristics of LDMC-WPT systems with resistive load when (a) ZPA at $x = 1$ and $x_{\min} = 0.5$, with different λ; and (b) ZPA at $x = x_{\min}$ and $x_{\min} = 0.5$, with different λ.

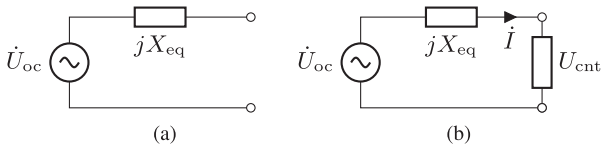

Fig. 8. (a) Thevenin equivalent circuit of a WPT system without a load and (b) with the addition of a battery load $U_{\rm cnt}$.

With (44)

$$U_{\rm oc} = -\frac{j^K x e_1 U_1 R}{b_2 x^2 + b_0}. \tag{49}$$

According to (18), (19), and $x = 1$, the expression of e_1 can be obtained as

$$e_1 = \pm\frac{\sqrt{P_{\rm a}}}{U_1\sqrt{R}}\sqrt{(a_2+a_0)^2+(b_2+b_0)^2}. \tag{50}$$

Combining (40), (42), (47), (49), and (50), the output power of the LDMC-WPT system with a battery load is

$$P_{\rm DC} = P_{\rm a}\cdot p_{\rm DC}(x) \tag{51}$$

where $p_{\rm DC}(x)$ is given by

$$p_{\rm DC}(x) = \sqrt{\frac{-b_2^2x^4+\left(a_2^2+2a_0a_2+a_0^2+b_2^2+b_0^2\right)x^2-b_0^2}{\left(a_2x^2+a_0\right)^2}}. \tag{52}$$

The maximum value of $p_{\rm DC}(x)$ is required to determine the maximum output power of the WPT system within a misalignment range. The derivative of $p_{\rm DC}^2(x)$ with respect to x is

$$\frac{d}{dx}p_{\rm DC}^2(x) = \frac{2x\left(A-Bx^2\right)}{\left(a_2x^2+a_0\right)^3} \tag{53}$$

where

$$\begin{aligned} A &= a_0^3+2a_0^2a_2+a_0a_2^2+a_0b_0^2+2a_2b_0^2+a_0b_2^2 \\ B &= a_0^2a_2+2a_0a_2^2+a_2^3+a_2b_0^2+2a_0b_2^2+a_2b_2^2. \end{aligned} \tag{54}$$

Let this derivative be equal to zero, then it can be deduced that when $x_{P_{\max}} = \sqrt{A/B}$, $p_{\rm DC}^2(x)$ reaches the maximum value given by the following equation (55) shown at the bottom of next page.

It is proved in Appendix D that when a_2, a_0, b_2, and b_0 satisfy (56), $p_{\rm DC}^2(x_{P_{\max}})$ has the minimum value as given in (57)

$$\frac{a_0}{a_2} = x_{\min},\quad \frac{b_0}{a_2} = \frac{\pm1\mp\lambda}{\sqrt{1-\lambda^2}}x_{\min}\quad \frac{b_2}{a_2} = \frac{\mp1\pm\lambda}{\sqrt{1-\lambda^2}} \tag{56}$$

$$\min\left[\,p_{\rm DC}^2\left(x_{P_{\max}}\right)\,\right] = \frac{x_{\min}^2+2\lambda x_{\min}+1}{2\left(1+\lambda\right)x_{\min}}. \tag{57}$$

And likewise, the analysis for WPT systems with odd-numbered current loops indicates that a_2, a_0, b_2, and b_0 have to satisfy the following to achieve the same minimum $p_{\rm DC}^2(x_{P_{\max}})$ in (57)

$$\frac{b_0}{b_2} = x_{\min},\quad \frac{a_0}{b_2} = \frac{\pm1\mp\lambda}{\sqrt{1-\lambda^2}}x_{\min}\quad \frac{a_2}{b_2} = \frac{\mp1\pm\lambda}{\sqrt{1-\lambda^2}}. \tag{58}$$

By substituting (56) into (52), the output power-misalignment characteristics after $\kappa_{\rm DC}$ is minimized can be derived as

$$p_{\rm DC}(x) = \sqrt{\frac{(\lambda-1)x^4+2(\lambda x_{\min}+x_{\min}^2+x_{\min}+1)x^2+(\lambda-1)x_{\min}^2}{\left(x^2+x_{\min}\right)^2\left(1+\lambda\right)}}. \tag{59}$$

Similarly, a fluctuation coefficient $\kappa_{\rm DC}$ can be defined as the ratio of the maximum output power in a certain misalignment range to the output power at the aligned position. The minimum value of $\kappa_{\rm DC}$ can be derived as

$$\kappa_{\rm DC,min}\left(x_{\min},\lambda\right) = \sqrt{\frac{x_{\min}^2+2\lambda x_{\min}+1}{2\left(1+\lambda\right)x_{\min}}}. \tag{60}$$

Comparing (60) with (26), it can be found that

$$\kappa_{\rm DC,min} = \sqrt{\kappa_R} < \kappa_R. \tag{61}$$

In summary, for an LDMC-WPT system with a battery load and given values of $x_{\min}$ (i.e., misalignment range) and λ, compared to that with a resistive load, the design of a_2, a_0, b_2, and b_0 enables a decrease and minimization of the fluctuation coefficient $\kappa_{\rm DC}$. Fig. 9 shows the output power-misalignment characteristics of an LDMC-WPT system with different $x_{\min}$ and λ. From Fig. 9, all $\kappa_{\rm DC}$ are minimized and much smaller than κ_R.

TABLE I
SUMMARY OF COEFFICIENTS FOR SOME REPORTED WPT SYSTEMS

Ref.	Topology	Current loops	a_2	b_2	a_0	b_0	$x_{\min}$	λ	κ_R	κ_{DC}	$\kappa_{\mathrm{DC,min}}$	γ	Notes
[15]	*CCC*	3	0	1.976	1	0	0.506	0	1.242	(1.242)	1.114	1.778	
[14]	X-type	3	0	2	1	0	0.5	0	1.2	(1.2)	1.095	1.803	
[17]	Three resonators	3	0	1.558	1	0	0.642	0	1.1	1.1	1.049	1.356	
[8]	*LCC*-S	3	0	1.778	1	0	0.562	0	1.17	1.17	1.082	1.574	90V output
[11]	S-SP	3	1.310	-0.304	0	1	0.744	-0.226	1.057	(1.075)	1.028	*	First setup
[13]	*LCC-LCC*	4	11.207	-1.621	6.273	1	0.561	0.955	1.088	(∞)	1.043	4.230	Case I
	S-*LCC*	3	1.949	-1.625	1.07	1	0.577	0.124	1.138	(∞)	1.067	*	Case I

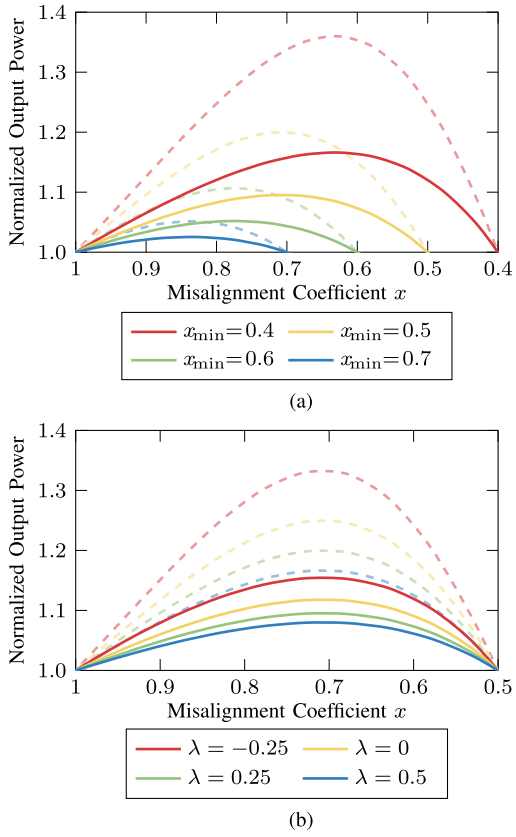

Fig. 9. Normalized output power-misalignment characteristics of the LDMC-WPT systems with battery load when κ_{DC} is minimized and (a) $\lambda = 0.25$ with different $x_{\min}$, (b) $x_{\min} = 0.5$ with different λ, and the comparison with systems with resistive load (dashed line).

E. Review

Table I summarized the coefficients of some WPT systems reported previously. a_2, b_2, a_0, b_0, $x_{\min}$, and λ are calculated either from the design parameters of the system or the measured parameters for experiments. Some κ_{DC} values are in brackets, which means experiments with a battery load are not conducted, and κ_{DC} is calculated according to the theory in Section III-D or simulation. For the last two systems, the calculated κ_{DC} is infinity, which means the output power will be very large at some positions within the desired misalignment range with a battery load. For γ of S-SP and S-*LCC* topologies, because ZPA is realized neither at the aligned position nor at the most misaligned position, this value is not calculated.

TABLE II
SPECIFICATIONS OF THE EXAMPLE WPT SYSTEM

Symbol	Parameter	Value
P_{a}	Power at aligned position	3.3 kW
U_{idc}	Input dc voltage	400 V
U_{odc}	Output dc voltage	400 V
R_{L}	AC load resistor	39.3 Ω
f	Operation frequency	85 kHz
$x_{\min}$	Minimum misalignment coefficient	0.5
λ		0.25

IV. DESIGN OF THE PROTOTYPE

In this article, an example two-coil WPT system is designed according to the above analysis, and the ZPA point is set at the aligned position. The design parameters are shown in Table II. In order to meet the design parameters of $x_{\min}$ and λ in Table II and minimize κ_{DC}, the above variables a_2, a_0, b_2, and b_0 should satisfy the three equations in (56). Furthermore, four loop currents $\dot{I}_{i\mathrm{a}}$ at the aligned position, which can be calculated by solving (5), are supposed to fulfill the following three conditions.

1) The input current is required to be in phase with the input voltage to realize ZPA.
2) The output current is capable of delivering the target power.
3) The current ratio of two coils at the aligned position or the most misaligned position is given.

For simplicity, the current ratio is set at 1 at the most misaligned position in this study. The above three conditions can be expressed as

$$\mathrm{Im}\left(\dot{I}_{1\mathrm{a}}\right) = 0,\ \left\|\dot{I}_{4\mathrm{a}}\right\|^2 R = P_{\mathrm{a}},\ \left\|\dot{I}_{2,x_{\min}}\right\| = \left\|\dot{I}_{3,x_{\min}}\right\|. \quad (62)$$

There are totally six equations in (56) and (62), and the circuit in Fig. 3 has exactly six unknown reactances to be solved. By solving (56) and (62), a two-coil WPT system is designed.

$$p_{\mathrm{DC}}^2\left(x_{P_{\max}}\right) = \frac{\left(a_2^2 + 2a_0a_2 + a_0^2 + b_2^2 - 2b_0b_2 + b_0^2\right)\left(a_2^2 + 2a_0a_2 + a_0^2 + b_2^2 + 2b_0b_2 + b_0^2\right)}{4\left(a_2 + a_0\right)\left(a_0^2a_2 + a_0a_2^2 + a_2b_0^2 + a_0b_2^2\right)}. \quad (55)$$

TABLE III
PARAMETERS OF THE COUPLER IN THE EXAMPLE WPT SYSTEM

Parameters		Value
Size of ferrites		500 mm × 500 mm × 5 mm
Size of shields		500 mm × 500 mm × 2 mm
Outer size of coils		450 mm × 450 mm
Inner size of coils		320 mm × 320 mm
Turns of coils		16
Clearance between shield and ferrite		3 mm
Clearance between ferrite and coil		3 mm
Airgap		175 mm
Litz wire	Strands	800
	Strand diameter	0.1 mm
	Wire diameter	3.9 mm
Inductance of the primary coil L_{P}		303.10 μH
Inductance of the secondary coil L_{S}		300.20 μH
Mutual inductance M_{a}		74.05 μH

* Transmitting and receiving pads are the same.

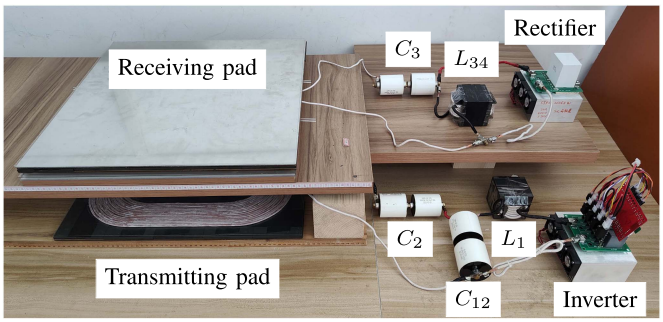

Fig. 10. Experimental setup of the prototype.

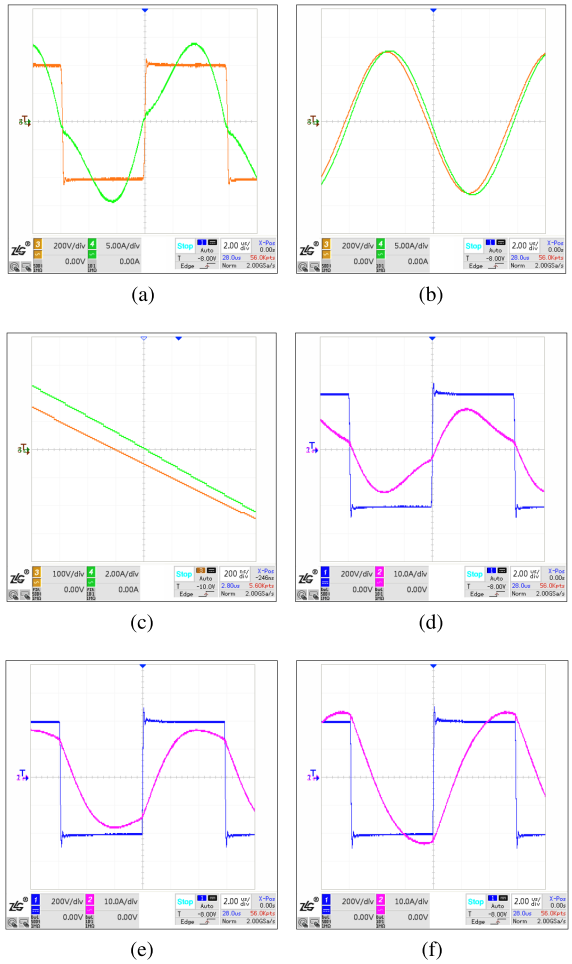

Fig. 11. Waveform of the input voltage (orange curves) and current (green curves) of the rectifier. (a) Original waveform, (b) waveform of a low-pass filter in the oscilloscope, and (c) zoom in of (b); and output voltage (blue curves) and current (pink curves) of the inverter at (d) 0 mm ($x = 1$); (e) 120 mm ($x = 0.705$); and (f) 170 mm ($x = 0.504$) with battery load.

The required specifications of the prototype are listed in Table II. Eventually, $\lambda = 0.25$ is chosen because it has a comparable flat output, as shown in Fig. 6(b), and has a comparable low input current, as shown in Fig. 7(a). Table III lists the parameters of the coupler of the prototype. By solving the six equations in (56) and (62), totally eight group of solutions for the compensating components in Fig. 3 can be obtained, as listed in Table IV. The input impedance of the last four groups within the misalignment range is capacitive, so they are discarded. From (62), all groups have the same coil currents, so only the losses of the compensating components need to be compared. By utilizing circuit simulation, the current values for each component can be determined. The prototype's capacitors are estimated to have a quality factor of 900, while the inductors possess a quality factor of 400. Table IV lists the computed losses, clearly indicating that the second group exhibits the lowest losses among the four groups.

V. EXPERIMENTAL VERIFICATION

In this section, a prototype, as shown in Fig. 10, is built according to the above design. The input voltage of the transmitter is generated by a full-bridge inverter, which consists of four C3M0021120D SiC MOSFETs from Cree. The output dc voltage is rectified by a full-bridge rectifier, which consists of four STPSC20065W SiC Schottky Diodes from STMicroelectronics. Table V lists the parameters of the compensating components.

However, higher harmonics still affect the phase difference between the input voltage and current of the rectifier. Fig. 11(a) shows the original waveforms and Fig. 11(b) shows the result after filtering with a low-pass filter in an oscilloscope. The phase difference can be measured, which is 6.88° (current lags voltage). Therefore, the load can be equivalent to an inductor in series with a resistor. The ac equivalent resistance is 39.3 Ω, so the reactance is 4.74 Ω, and the load inductance can be calculated as 8.88 μH. This equivalent inductance can basically replace X_4 (11.09 μH). Thus, a lumped inductor in the position of X_4 is not necessary in the prototype.

After measurement, the maximum misalignment distance corresponding to $x_{\min} = 0.5$ is 170 mm. Fig. 12 shows the change of the output power with misalignment coefficient x under the resistive load and the battery load. The measured output power is in good agreement with the theoretical value. The measured fluctuation coefficient $\kappa_{R,\mathrm{exp.}}$ and $\kappa_{\mathrm{DC,exp.}}$ are

TABLE IV
SOLUTIONS OF THE SIX COMPENSATING COMPONENTS FOR THE PROTOTYPE

	X_1		X_{12}		X_2		X_3		X_{34}		X_4		Loss of
	Type	Value	Type	Value	Type	Value	Type	Value	Type	Value	Type	Value	components
1	C	13.35 nF	L	167.69 μH	C	5.06 nF	C	10.10 nF	L	83.84 μH	L	11.09 μH	124.66 W
2	L	72.75 μH	C	20.91 nF	C	9.81 nF	C	10.10 nF	L	83.84 μH	L	11.09 μH	64.61 W
3	C	13.35 nF	L	167.69 μH	C	5.06 nF	C	19.24 nF	C	41.82 nF	L	178.78 μH	141.16 W
4	L	72.75 μH	C	20.91 nF	C	9.81 nF	C	19.24 nF	C	41.82 nF	L	178.78 μH	108.31 W
5	C	48.19 nF	L	167.69 μH	C	14.10 nF	C	8.33 nF	L	83.84 μH	C	19.61 nF	*
6	L	262.62 μH	C	20.91 nF	L	86.74 μH	C	8.33 nF	L	83.84 μH	C	19.61 nF	*
7	C	48.19 nF	L	167.69 μH	C	14.10 nF	C	13.68 nF	C	41.82 nF	C	316.16 nF	*
8	L	262.62 μH	C	20.91 nF	L	86.74 μH	C	13.68 nF	C	41.82 nF	C	316.16 nF	*

TABLE V
PARAMETERS OF THE COMPENSATING COMPONENTS OF THE PROTOTYPE

Value		Value	
L_1	74.53 μH	C_3	10.30 nF
C_{12}	20.78 nF	L_{34}	84.42 μH
C_2	9.69 nF	(L_4)	(10.75 μH)

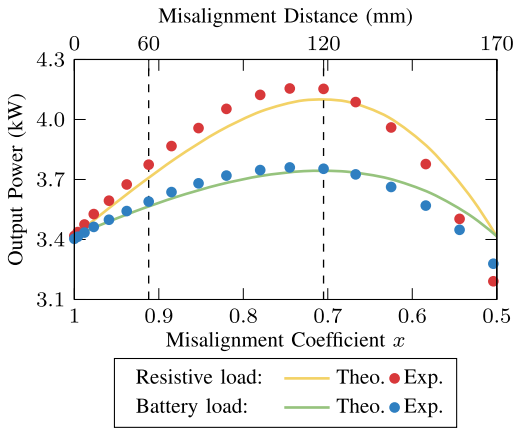

Fig. 12. Output power versus misalignment coefficient x.

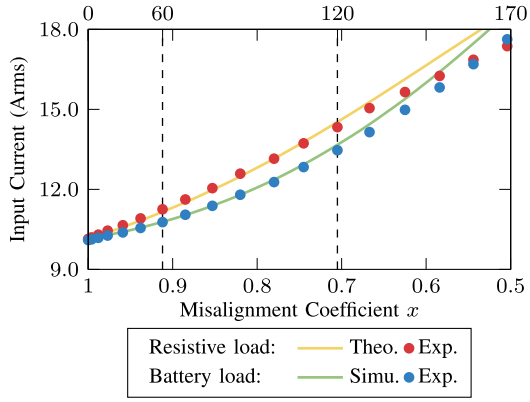

Fig. 13. Input current versus misalignment coefficient x.

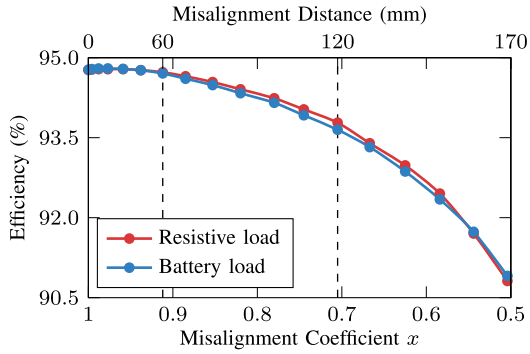

Fig. 14. Efficiency versus misalignment coefficient x.

1.216 and 1.105, with the resistive load and the battery load, respectively. The waveforms of the inverter's output voltage and current are given in Fig. 11(d)–(f). At the aligned position, the voltage and current are basically in phase. As the misalignment increases, the input current also rises, and ZVS is realized in the whole misalignment range. Fig. 13 shows that the input current increases with decreasing x, from which the measured fluctuation coefficient is 1.746. Figs. 12 and 13 contain several discrepancies, potentially stemming from errors in compensating components, the parasitic resistance of both the compensating components and coils, variations in coils' self-inductance following coupling adjustments, and measurement inaccuracies in mutual inductance. Nonetheless, the overall trend observed in the theoretical values remains consistent with the experimental measurements.

Generally, a larger input current is expected when the misalignment becomes larger. Fig. 14 shows the efficiency variation in the misalignment range. At the aligned position, the dc–dc efficiency of the prototype is 94.8%, and at the most misaligned position, i.e., 170 mm, the efficiency drops to 90.9%.

VI. CONCLUSION

This article provides a general analysis of the misalignment characteristics of fixed-frequency WPT systems. It presents circuit and mathematical models for WPT systems with different numbers of coils, which are categorized based on their output current-misalignment characteristics. The study analyzes the output current/power- and input current-misalignment characteristics of LDMC-WPT systems with either a resistive load or a battery load. It is demonstrated that a smoother power fluctuation could be achieved by a battery load compared with a resistive load. Essentially, all low-degree WPT systems can be designed with the help of the general model presented in this article. A design example of a 3.3 kW two-coil WPT prototype is included.

The experimental results support the presented theory well. In addition, this article introduces the concept of the HDMC-WPT system, for the first time, which might outperform LDMC-WPT systems in terms of misalignment characteristics.

Appendix A

The determinant of a square matrix of degree K is defined as

$$\sum \mathrm{sgn}(p_1,\ldots,p_K)a_{1p_1},\ldots,a_{Kp_K} \tag{A1}$$

where $p_1,\ldots,p_K$ is a permutation of $1,\ldots,K$, and $\mathrm{sgn}(p_1,\ldots,p_K)$ is the sign of the permutation. To count the degrees of x in $\det(\boldsymbol{Z}_{m\sim n})$ and $\det(\boldsymbol{A}_{1K})$, we only need to consider the product $a_{1p_1},\ldots,a_{Kp_K}$ in (A1). This corresponds to the product of elements in different rows and different columns of a square matrix.

In (9), if l elements are chosen from matrix-$\boldsymbol{M}$ in (6) for $a_{1p_1},\ldots,a_{Kp_K}$, then $(m-l)$ elements, excluding the first row (if it exists), must be chosen from the matrix $\boldsymbol{P}$. If the first row of $\boldsymbol{P}$ is included, then one of its elements must be chosen because all elements in the first row of $\boldsymbol{M}$ are zero, resulting in a selection of $(m+1-l)$ elements from $\boldsymbol{P}$. Similarly, the first column of $\boldsymbol{P}$ must have one of its elements chosen, leading to a selection of $(m-l)$ elements from $\boldsymbol{P}$, except for the first column (if it exists). This selection process leads to the choice of l elements from $\boldsymbol{M}^{\mathrm{T}}$ as well. Since l elements are selected from both $\boldsymbol{M}$ and $\boldsymbol{M}^{\mathrm{T}}$, and l can take values from 0 to the smaller of m and n, the exponent of x in $\det(\boldsymbol{Z}_{m\sim n})$ will be an even number ranging from 0 to $2\cdot\min(m,n)$. Furthermore, the element $(jS_{00}+R)$ located at the lower left corner of the matrix is a complex number. Therefore, the coefficient of x^{2l} in the expansion of the determinant can be defined as the complex number $(a_{2l}+jb_{2l})$. In summary, the general expression of $\det(\boldsymbol{Z}_{m\sim n})$ can be written as (14).

The proof method for $\det(\boldsymbol{A}_{1K})$ is similar to the above. Matrix $\boldsymbol{A}_{1K}$ can be expressed as

$$\left[\begin{array}{cccc|ccc|c}
jP_{01} & jP_{11} & \cdots & jP_{1m} & xj\omega M_{1n} & \cdots & xj\omega M_{12} & xj\omega M_{11} \\
jP_{02} & jP_{12} & \cdots & jP_{2m} & xj\omega M_{2n} & \cdots & xj\omega M_{22} & xj\omega M_{12} \\
\vdots & \vdots & \ddots & \vdots & \vdots & \ddots & \vdots & \vdots \\
jP_{0m} & jP_{1m} & \cdots & jP_{mm} & xj\omega M_{mn} & \cdots & xj\omega M_{m2} & xj\omega M_{m1} \\
\hline
0 & xj\omega M_{1n} & \cdots & xj\omega M_{mn} & jS_{nn} & \cdots & jS_{2n} & jS_{1n} \\
\vdots & \vdots & \ddots & \vdots & \vdots & \ddots & \vdots & \vdots \\
0 & xj\omega M_{11} & \cdots & xj\omega M_{m1} & jS_{1n} & \cdots & jS_{12} & jS_{11} \\
0 & 0 & \cdots & 0 & jS_{0n} & \cdots & jS_{02} & jS_{01}
\end{array}\right] \tag{A2}$$

If l elements in the block matrix in the upper right corner are selected, then $(m-l)$ elements (if the first row is included) or $(m-l-1)$ elements (if the first row is not included) in the block matrix in the upper left corner are supposed to be selected. If the first column is included, an element in it must be selected, so $(m-l-1)$ elements in the remain are supposed to be selected. Thus, $(l+1)$ elements should be selected in the block matrix in the lower left corner. As a result, the power of x in $\det(\boldsymbol{A}_{1K})$ is odd number. In addition, since all elements are pure imaginary numbers, matrix $\boldsymbol{A}_{1K}$, j in each row can be extracted as $j^{(K-1)}$ and then put in the front, and the coefficient of $x^{(2l-1)}$ is a real number. In summary, the general expression of $\det(\boldsymbol{A}_{1K})$ can be written as (13).

Appendix B

Both multicoil-to-single-coil and single-coil-to-multicoil WPT systems are supposed to be considered. In the former case, $\boldsymbol{Z}_{m\sim n}$ in (28) should be $\boldsymbol{Z}_{m\sim 1}$ shown in (B1), as well as $\boldsymbol{A}_{11}$ in (28) should be $\boldsymbol{A}_{11,m\sim 1}$ by deleting the first row and first column of $\boldsymbol{Z}_{m\sim 1}$. And it is similar for the latter case, with $\boldsymbol{Z}_{1\sim n}$ in (B2) and $\boldsymbol{A}_{11,1\sim n}$ instead. Any of the four determinants $\det(\boldsymbol{Z}_{m\sim 1})$, $\det(\boldsymbol{A}_{11,m\sim 1})$, $\det(\boldsymbol{Z}_{1\sim n})$, and $\det(\boldsymbol{A}_{11,1\sim n})$ can be divided into the sum of two determinants with the form on the left side of the equal sign in (B11), as shown in (B3), (B5), (B7), and (B9a), respectively. Equation (B11) is a method for calculating the determinant of a block matrix

$$\begin{vmatrix} \boldsymbol{V} & \boldsymbol{O} \\ \boldsymbol{O} & \boldsymbol{W} \end{vmatrix} = |\boldsymbol{V}|\cdot|\boldsymbol{W}|. \tag{B11}$$

According to the above method, light cyan block and light purple block in (B3) can be simplified to (B4a), as well as light magenta block and the whole equation in (B3) can be simplified to and (B4b), where the meaning of $\oplus$ is exclusive or. Then, (B5) can be simplified to (B6a) and (B6b). Similarly, light purple block and light magenta block in (B7) can be simplified to (B8a) as well as light cyan block and the whole equation can be simplified to (B8b). And (B9a) and (B9b) can be simplified to (B10a) and (B10a), respectively. In these equations, A_1, B_1, A_2, B_2, C, D, E, and F are real numbers calculated from their corresponding blocks in determinants. By comparing (B4a) with (B6a), it can be found that for the two coefficients of x^2 in these equations, the ratio is purely imaginary, and for the remaining coefficients, the ratio is the same, which also applies to (B4b) and (B6b), (B8a) and (B10a)(no x^2-term in this equation however), and (B8b) and (B10b). The above analysis can be written as (29).

Appendix C

The determinants of $\boldsymbol{Z}_{m\sim 1}$ in (B1) and $\boldsymbol{Z}_{1\sim n}$ in (B2) can be rewritten in the following form:

$$\det(\boldsymbol{Z}) = \begin{vmatrix} jt_{11} & \cdots & jt_{1(n-1)} & jt_{1n} \\ \vdots & \ddots & \vdots & \vdots \\ jt_{1(n-1)} & \cdots & jt_{(n-1)(n-1)} & jt_{(n-1)n} \\ jt_{1n} & \cdots & jt_{(n-1)n} & jt_{nn}+R \end{vmatrix} \tag{C1}$$

where t_{ij} are the real numbers.

$\boldsymbol{Z}_{m\sim1}=$

$$\left[\begin{array}{ccccc|c} jP_{00} & jP_{01} & \cdots & jP_{0m} & 0 & 0 \\ jP_{01} & jP_{11} & \cdots & jP_{1m} & xj\omega M_1 & 0 \\ \vdots & \vdots & \ddots & \vdots & \vdots & \vdots \\ jP_{0m} & jP_{1m} & \cdots & jP_{mm} & xj\omega M_m & 0 \\ \hline 0 & xj\omega M_1 & \cdots & xj\omega M_m & jS_{11}+(R) & jS_{01} \\ 0 & 0 & \cdots & 0 & jS_{01} & jS_{00}+(R) \end{array}\right] \tag{B1}$$

$\boldsymbol{Z}_{1\sim n}=$

$$\left[\begin{array}{cc|ccc|c} jP_{00} & jP_{01} & 0 & \cdots & 0 & 0 \\ jP_{01} & jP_{11} & xj\omega M_1 & \cdots & xj\omega M_n & 0 \\ \hline 0 & xj\omega M_1 & jS_{nn} & \cdots & jS_{1n} & jS_{0n} \\ \vdots & \vdots & \vdots & \ddots & \vdots & \vdots \\ 0 & xj\omega M_n & jS_{1n} & \cdots & jS_{11}+(R) & jS_{01} \\ 0 & 0 & jS_{0n} & \cdots & jS_{01} & jS_{00}+(R) \end{array}\right] \tag{B2}$$

$\det(\boldsymbol{Z}_{m\sim1})=$

$$\left|\begin{array}{ccccc|c} jP_{00} & jP_{01} & \cdots & jP_{0m} & 0 & 0 \\ jP_{01} & jP_{11} & \cdots & jP_{1m} & xj\omega M_1 & 0 \\ \vdots & \vdots & \ddots & \vdots & \vdots & \vdots \\ jP_{0m} & jP_{1m} & \cdots & jP_{mm} & xj\omega M_m & 0 \\ 0 & xj\omega M_1 & \cdots & xj\omega M_m & 0 & 0 \\ \hline 0 & 0 & \cdots & 0 & 0 & jS_{00}+(R) \end{array}\right| + \left|\begin{array}{ccccc|c} jP_{00} & jP_{01} & \cdots & jP_{0m} & 0 & 0 \\ jP_{01} & jP_{11} & \cdots & jP_{1m} & 0 & 0 \\ \vdots & \vdots & \ddots & \vdots & \vdots & \vdots \\ jP_{0m} & jP_{1m} & \cdots & jP_{mm} & 0 & 0 \\ \hline 0 & 0 & \cdots & 0 & jS_{11}+(R) & jS_{01} \\ 0 & 0 & \cdots & 0 & jS_{01} & jS_{00}+(R) \end{array}\right| \tag{B3}$$

$$\det(\boldsymbol{Z}_{m\sim1}) = j^{(m+1)\oplus(m+2)}\cdot A_1\cdot x^2 + j^{m\oplus(m+1)}\cdot B_1\cdot(jS_{11}+R) \tag{B4a}$$

$$\det(\boldsymbol{Z}_{m\sim1}) = j^{(m+1)\oplus(m+2)}\cdot A_1\cdot(jS_{00}+R)\cdot x^2 + j^{m\oplus(m+1)}\cdot B_1\cdot\left(S_{01}^2 - S_{00}S_{11} + jS_{11}R\right) \tag{B4b}$$

$$\det(\boldsymbol{A}_{11,m\sim1})=\left|\begin{array}{ccccc|c} jP_{11} & \cdots & jP_{1m} & xj\omega M_1 & 0 \\ \vdots & \ddots & \vdots & \vdots & \vdots \\ jP_{1m} & \cdots & jP_{mm} & xj\omega M_m & 0 \\ xj\omega M_1 & \cdots & xj\omega M_m & 0 & 0 \\ \hline 0 & \cdots & 0 & 0 & jS_{00}+(R) \end{array}\right| + \left|\begin{array}{ccccc|c} jP_{11} & \cdots & jP_{1m} & 0 & 0 \\ \vdots & \ddots & \vdots & \vdots & \vdots \\ jP_{1m} & \cdots & jP_{mm} & 0 & 0 \\ \hline 0 & 0 & 0 & jS_{11}+(R) & jS_{01} \\ 0 & 0 & 0 & jS_{01} & jS_{00}+(R) \end{array}\right| \tag{B5}$$

$$\det\left(\boldsymbol{A}_{11,m\sim1}\right) = j^{m\oplus(m+1)}A_2\cdot x^2 + j^{(m-1)\oplus m}B_2\left(jS_{11}+R\right) \tag{B6a}$$

$$\det\left(\boldsymbol{A}_{11,m\sim1}\right) = j^{m\oplus(m+1)}A_2\cdot(jS_{00}+R)\cdot x^2 + j^{(m-1)\oplus m}B_2\left(S_{01}^2 - S_{00}S_{11} + jS_{11}R\right) \tag{B6b}$$

$\det(\boldsymbol{Z}_{1\sim n})=$

$$\left|\begin{array}{c|cccc|c} jP_{00} & 0 & 0 & \cdots & 0 & 0 \\ \hline 0 & 0 & xj\omega M_n & \cdots & xj\omega M_1 & 0 \\ 0 & xj\omega M_n & jS_{nn} & \cdots & jS_{1n} & jS_{0n} \\ \vdots & \vdots & \vdots & \ddots & \vdots & \vdots \\ 0 & xj\omega M_1 & jS_{1n} & \cdots & jS_{11}+(R) & jS_{01} \\ 0 & 0 & jS_{0n} & \cdots & jS_{01} & jS_{00}+(R) \end{array}\right| + \left|\begin{array}{cc|ccc|c} jP_{00} & jP_{01} & 0 & \cdots & 0 & 0 \\ jP_{01} & jP_{11} & 0 & \cdots & 0 & 0 \\ \hline 0 & 0 & jS_{nn} & \cdots & jS_{1n} & jS_{0n} \\ \vdots & \vdots & \vdots & \ddots & \vdots & \vdots \\ 0 & 0 & jS_{1n} & \cdots & jS_{11}+(R) & jS_{01} \\ 0 & 0 & jS_{0n} & \cdots & jS_{01} & jS_{00}+(R) \end{array}\right| \tag{B7}$$

$$\det(\boldsymbol{Z}_{1\sim n}) = (C+jD)\cdot x^2 + jP_{11}\cdot(E+jF) \tag{B8a}$$

$$\det(\boldsymbol{Z}_{1\sim n}) = jP_{00}\cdot(C+jD)\cdot x^2 + \left(P_{01}^2 - P_{00}P_{11}\right)\cdot(E+jF) \tag{B8b}$$

$$\det\left(\boldsymbol{A}_{11,1\sim n}\right) = \left|\begin{array}{ccccc} 0 & xj\omega M_1 & \cdots & xj\omega M_n & 0 \\ xj\omega M_1 & jS_{nn} & \cdots & jS_{1n} & jS_{0n} \\ \vdots & \vdots & \ddots & \vdots & \vdots \\ xj\omega M_n & jS_{1n} & \cdots & jS_{11}+(R) & jS_{01} \\ 0 & jS_{0n} & \cdots & jS_{01} & jS_{00}+(R) \end{array}\right| + \left|\begin{array}{c|cccc} jP_{11} & 0 & \cdots & 0 & 0 \\ \hline 0 & jS_{nn} & \cdots & jS_{1n} & jS_{0n} \\ \vdots & \vdots & \ddots & \vdots & \vdots \\ 0 & jS_{1n} & \cdots & jS_{11}+(R) & jS_{01} \\ 0 & jS_{0n} & \cdots & jS_{01} & jS_{00}+(R) \end{array}\right| \tag{B9a}$$

$$\det\left(\boldsymbol{A}_{11,1\sim n}\right) = \left|\begin{array}{ccc} jS_{nn} & \cdots & jS_{1n} & jS_{0n} \\ \vdots & \ddots & \vdots & \vdots \\ jS_{1n} & \cdots & jS_{11}+(R) & jS_{01} \\ jS_{0n} & \cdots & jS_{01} & jS_{00}+(R) \end{array}\right| \tag{B9b}$$

$$\det\left(\boldsymbol{A}_{11,1\sim n}\right) = (E+jF) \tag{B10a}$$

$$\det\left(\boldsymbol{A}_{11,1\sim n}\right) = (C+jD)\cdot x^2 + jP_{11}\cdot(E+jF) \tag{B10b}$$

This determinant can be considered as the sum of two determinants, i.e.,

$$\begin{aligned}&\det(\boldsymbol{Z})\\&=\begin{vmatrix} jt_{11} & \cdots & jt_{1n}\\ \vdots & \ddots & \vdots\\ jt_{1n} & \cdots & jt_{nn}\end{vmatrix}\\&+\begin{vmatrix} jt_{11} & \cdots & jt_{1(n-1)} & jt_{1n}\\ \vdots & \ddots & \vdots & \vdots\\ jt_{1(n-1)} & \cdots & jt_{(n-1)(n-1)} & jt_{(n-1)n}\\ 0 & \cdots & 0 & R\end{vmatrix}\end{aligned} \tag{C2}$$

Then

$$\det(\boldsymbol{Z}) = j^n T_1 + j^{(n-1)} T_2 \cdot R \tag{C3}$$

where T_1 and T_2 are the real numbers.

It can be found that if the number of current loops is an even number, then the first term is a real number, and the second is an imaginary number. Thus, the real part of $\det(\boldsymbol{Z})$ is independent of R and the imaginary part is linearly proportional to R. From (15)

$$\det(\boldsymbol{Z}) = \left(a_2 x^2 + a_0\right) + j\left(b_2 x^2 + b_0\right). \tag{C4}$$

Therefore

$$b_2 x^2 + b_0 = T_2 R. \tag{C5}$$

Thus, b_2 and b_0 should be linearly proportional to R, as shown in (44). As a result, (43) can be obtained. And likewise, if the number of current loops is an odd number, then the real part of $\det(\boldsymbol{Z})$ is proportional to R and the imaginary part is independent of R, as shown in (46). And (45) can be obtained.

Appendix D

According to $x_{\min}$ in (21) and λ in (23), (55) can be transformed into

$$p_{\mathrm{DC}}^2\left(x_{P_{\max}}\right) = \frac{1}{4}\cdot\left(x_{\min}^2 + 2\lambda x_{\min} + 1\right)\cdot F \tag{D1}$$

where

$$F = \frac{\left(a_2^2 + b_2^2\right)\left(a_2^2 + 2a_0a_2 + a_0^2 + b_2^2 - 2b_0b_2 + b_0^2\right)}{\left(a_2 + a_0\right)\left(a_0^2a_2 + a_0a_2^2 + a_2b_0^2 + a_0b_2^2\right)}. \tag{D2}$$

Therefore, for the minimum value of (55), only the minimum of F is required. Set k_1, k_2, and k_3 as

$$k_1 = \frac{a_0}{a_2},\quad k_2 = \frac{b_0}{a_2},\quad k_3 = \frac{b_2}{a_2}. \tag{D3}$$

According to (21) and (23)

$$k_2 = \frac{\pm x_{\min} \mp \lambda k_1}{\sqrt{1-\lambda^2}},\quad k_3 = \frac{\mp k_1 \pm \lambda x_{\min}}{x_{\min}\sqrt{1-\lambda^2}}. \tag{D4}$$

Substituting (D4) into (D2), $F(k_1)$ as a function of k_1 can be deduced as

$$F(k_1) = \frac{\begin{array}{c}\left({k_1}^2 + {x_{\min}}^2\right)\left({x_{\min}}^2 - 2\lambda x_{\min} + 1\right)\\ -2k_1x_{\min}\left(\lambda {x_{\min}}^2 - 2x_{\min} + \lambda\right)\end{array}}{{x_{\min}}^2\left(1-\lambda^2\right)\left(1+k_1\right)\left(k_1 + {x_{\min}}^2\right)}. \tag{D5}$$

Taking the derivative of $F(k_1)$, then

$$F'(k_1) = \frac{\left({k_1}^2 - x_{\min}^2\right)\left(x_{\min}^2 - 1\right)^2}{x_{\min}^2\left(1-\lambda^2\right)\left(1+k_1\right)^2\left(k_1 + x_{\min}^2\right)^2}. \tag{D6}$$

Let $F'(k_1)$ be equal to zero, the value of k_1 can be calculated as $\pm x_{\min}$. But $F(-x_{\min})$ in (D7) is less than zero and requires rounding off. Therefore, $k_1 = x_{\min}$ is selected

$$F(x_{\min}) = \frac{2}{\left(1+\lambda\right)x_{\min}},\quad F(-x_{\min}) = -\frac{2}{\left(1-\lambda\right)x_{\min}}. \tag{D7}$$

Substituting $F(x_{\min})$ into (D1), (60) can be obtained.

References

[1] "Wireless power transfer for light-duty plug-in/electric vehicles and alignment methodology," *Standard SAE Int*, Warrendale, PA, USA, Aug. 2022.

[2] M. Budhia, J. T. Boys, G. A. Covic, and C.-Y. Huang, "Development of a single-sided flux magnetic coupler for electric vehicle IPT charging systems," *IEEE Trans. Ind. Electron.*, vol. 60, no. 1, pp. 318–328, Jan. 2013.

[3] Y. Chen, R. Mai, Y. Zhang, M. Li, and Z. He, "Improving misalignment tolerance for IPT system using a third-coil," *IEEE Trans. Power Electron.*, vol. 34, no. 4, pp. 3009–3013, Apr. 2019.

[4] G. Yang, S. Dong, C. Zhu, R. Lu, G. Wei, and K. Song, "Design of a high lateral misalignment tolerance magnetic coupler for wireless power transfer systems," in *Proc. IEEE PELS Workshop Emerg. Technol., Wireless Power Transf.*, 2017, pp. 34–39.

[5] Z. Yao et al., "Minimizing current in inductive power transfer systems with an asymmetrical factor for misalignment tolerance and wide load range," *IEEE Trans. Power Electron.*, vol. 36, no. 9, pp. 9886–9896, Sep. 2021.

[6] V.-B. Vu et al., "Operation of inductive charging systems under misalignment conditions: A review for electric vehicles," *IEEE Trans. Transport. Electrific.*, vol. 9, no. 1, pp. 1857–1887, Mar. 2023.

[7] H. Feng, T. Cai, S. Duan, X. Zhang, H. Hu, and J. Niu, "A dual-side-detuned series–series compensated resonant converter for wide charging region in a wireless power transfer system," *IEEE Trans. Ind. Electron.*, vol. 65, no. 3, pp. 2177–2188, Mar. 2018.

[8] H. Feng, T. Cai, S. Duan, J. Zhao, X. Zhang, and C. Chen, "An LCC-compensated resonant converter optimized for robust reaction to large coupling variation in dynamic wireless power transfer," *IEEE Trans. Ind. Electron.*, vol. 63, no. 10, pp. 6591–6601, Oct. 2016.

[9] W. Li, W. Mei, Q. Yuan, Y. Song, Z. Dongye, and L. Diao, "Detuned resonant capacitors selection for improved misalignment tolerance of LCC-S compensated wireless power transfer system," *IEEE Access*, vol. 10, pp. 49474–49484, 2022.

[10] D. Shen, G. Du, W. Zeng, Z. Yang, and J. Li, "Research on optimization of compensation topology parameters for a wireless power transmission system with wide coupling coefficient fluctuation," *IEEE Access*, vol. 8, pp. 59648–59658, 2020.

[11] Y. Yao, Y. Wang, X. Liu, K. Lu, and D. Xu, "Analysis and design of an S/SP compensated IPT system to minimize output voltage fluctuation versus coupling coefficient and load variation," *IEEE Trans. Veh. Technol.*, vol. 67, no. 10, pp. 9262–9272, Oct. 2018.

[12] J. Hou, Q. Chen, Z. Zhang, S.-C. Wong, and C. K. Tse, "Analysis of output current characteristics for higher order primary compensation in inductive power transfer systems," *IEEE Trans. Power Electron.*, vol. 33, no. 8, pp. 6807–6821, Aug. 2018.

[13] A. Ramezani and M. Narimani, "Optimized electric vehicle wireless chargers with reduced output voltage sensitivity to misalignment," *IEEE Trans. Emerg. Sel. Topics Power Electron.*, vol. 8, no. 4, pp. 3569–3581, Dec. 2020.

[14] H. Feng, A. Dayerizadeh, and S. M. Lukic, "A coupling-insensitive X-type IPT system for high position tolerance," *IEEE Trans. Ind. Electron.*, vol. 68, no. 8, pp. 6917–6926, Aug. 2021.

[15] J. Zhao, T. Cai, S. Duan, H. Feng, C. Chen, and X. Zhang, "A general design method of primary compensation network for dynamic WPT system maintaining stable transmission power," *IEEE Trans. Power Electron.*, vol. 31, no. 12, pp. 8343–8358, Dec. 2016.

[16] Y. Yao, Y. Wang, X. Liu, Y. Pei, D. Xu, and X. Liu, "Particle swarm optimization-based parameter design method for S/CLC-compensated IPT systems featuring high tolerance to misalignment and load variation," *IEEE Trans. Power Electron.*, vol. 34, no. 6, pp. 5268–5282, Jun. 2019.

[17] Y. Yao, A. U. Ibrahim, and W. Zhong, "A three-resonator wireless power transfer system with constant-output feature within a misalignment range," *IEEE Trans. Power Electron.*, vol. 37, no. 12, pp. 15753–15763, Dec. 2022.

[18] C. K. Alexander and M. N. O Sadiku,*Fundamentals of Electric Circuits*. New York, NY, USA: McGraw-Hill Higher Education, 2007.

Yixiang Yao was born in Shanxi Province, China, in 1997. He received the B.Eng. degree in electrical engineering and automation from Xi'an Jiaotong University, Xi'an, China, in 2019. He is currently working toward the Ph.D. degree in electrical engineering with Zhejiang University, Hangzhou, China.

His current research interests include wireless power transfer technologies and power electronics.

Wenxing Zhong (Senior Member, IEEE) received the B.Eng. degree in electrical engineering from Tsinghua University, Beijing, China, in 2007, and the Ph.D. degree from the City University of Hong Kong, Hong Kong, in 2012.

He is currently a Professor with the Department of Electrical Engineering, Zhejiang University, Hangzhou, China. From March 2016 to May 2017, he was a Research Assistant Professor with the Department of Electrical and Electronic Engineering, University of Hong Kong, Hong Kong. His research interests include wireless power transfer and power electronics.

Dr. Zhong was a recipient of two Transactions First Prize Paper Awards from the IEEE Power Electronics Society.